Non-Adaptive Speed and Position Estimation of Doubly-Fed Induction Generator in Grid-Connected Operations

Marcin Morawiec, *Senior Member, IEEE*, and Krzysztof Blecharz

***Abstract*—The nonadaptive speed and position estimation scheme for a doubly-fed induction generator (DFIG) is presented in this article. The observer structure is based on the extension of the mathematical model of DFIG to the introduced H vector. Based on the defined H vector, the nonadaptive position and speed estimation is proposed. The Lyapunov method is extended to the practical stability theorem to stabilize the structure. The classic stator field-oriented control to active and reactive power control is used in the sensorless control system. The performance of the proposed algorithm of the speed and position observer is validated by simulation and experimental results using the 2 kW generator. The comparison tests to the classical model reference adaptive system based observer are provided. Finally, the article contains a summary in which the non-adaptive speed estimation is discussed in context to the adaptive reconstruction of the rotor speed and position.**

***Index Terms*—Doubly fed induction generator (DFIG), sensorless control, state observer.**

NOMENCLATURE

$i_{sx,y}$	Stator current vector components.
$i_{rx,y}$	Stator current vector components.
$u_{r\alpha,\beta}$	Rotor voltage vector components.
$u_{s\alpha,\beta}$	Stator voltage vector components.
ω_r	Rotor angular speed.
θ_r	Rotor position.
R_r, R_s	Rotor and stator resistances.
L_m	Mutual-flux inductance.
L_s, L_r	Stator and rotor inductances.
T_e	Electromagnetic torque.
T_L	Load torque.
J	Machine torque of inertia.
τ	Relative time.
$\hat{\theta}_r$	Estimated rotor position.
$\hat{\omega}_r$	Estimated rotor electrical speed.
$\tilde{\omega}_r$	Rotor speed error.
$\tilde{\theta}_r$	Rotor position error.
"^"	Estimated values.
"$\sim$"	Error of estimated values.
(x, y)	Coordinate system associated with any angular speed.

Manuscript received 15 September 2022; revised 8 February 2023 and 14 April 2023; accepted 10 May 2023. Date of publication 30 May 2023; date of current version 27 October 2023. *(Corresponding author: Marcin Morawiec.)*

The authors are with the Institute of Automatic Control of Electric Drives, Gdansk University of Technology, 80-233 Gdansk, Poland (e-mail: marcin.morawiec@pg.edu.pl; krzysztof.blecharz@pg.edu.pl).

Color versions of one or more figures in this article are available at https://doi.org/10.1109/TIE.2023.3279548.

Digital Object Identifier 10.1109/TIE.2023.3279548

I. INTRODUCTION

THE doubly-fed induction generator (DFIG) is one of the most used constructions in high-power wind power plants due to a few advantageous features. A generator of this type enables the wind turbine to operate a wide range of changes in the rotational speed of the shaft to improve the efficiency of energy production from wind. The power of the rotor-side converter is only a fraction of the power of the generator. Other advantages of the system are high precision control of active and reactive power and good quality power transferred to the power grid. A high-performance generator system has to use advanced control methods. Generator control techniques in different are generally reported based on known vector control methods, such as field-oriented control [1], [2], [3], direct power [4], [5] or torque control [6], and nonlinear control [7], [8], [9]. In all the above-mentioned control techniques, information about the generator shaft position and its angular velocity is necessary for the implementation of the control system. Measurement of the generator rotor position with the use of the most popular solution in the form of a mechanical rotary motion sensor causes technical difficulties in its assembly and significantly reduces the reliability of the entire system. Therefore, in advanced electric drive control systems, a tendency can be observed to eliminate the speed sensor and replace it with algorithmic solutions. This approach, known as sensorless, can significantly increase the reliability of the control system and reduce the wiring of the system. Another important aspect of the application of sensorless algorithms is their use for diagnostics of generator operation. The least complicated technique is the algorithms operating in an open calculation loop [10], [11], where the rotor position angle is determined based on the measured and calculated value of the stator or rotor current in a specific coordinate system. These algorithms are sensitive to changes in machine parameters and measurement noise due to no error correction mechanism.

The model reference adaptive system (MRAS) algorithm is the most numerous group of solutions for estimating the shaft angle and selected generator state variables. Depending on the adopted mathematical model of the generator and the

working variables, the MRAS algorithm takes various variants, the most important being stator flux (SF-MRAS) [12], rotor or stator current (RC-MRAS) [13], and back electromotive force (EMF-MRAS) model [14]. In general, the operation of MRAS algorithms, depending on the choice of the reference model structure and the error correction mechanism, is sensitive to the operation of the generator system near a low slip frequency. A different solution is shown in [15], [16], where rotor angle estimation is realized by the applications of the second-order generalized integrator and frequency-locked loop structures to filtered rotor current in the sensorless generator control system connected to the power grid. The correctness of the algorithm operation is related to the limited dynamics of the machine shaft speed change [17].

In [18] and [19], the authors present a method for estimating velocity and angle using a high-order sliding mode observer and a phase-locked loop. The operation of this algorithm is based on accurate, current measurements. Considering the assumed sliding plane, the error of the observer's correction oscillates around minimal values, which may affect the estimation accuracy. Another algorithm approach is the high-frequency method [20], [21], whereby a high-frequency current or voltage signal is injected on the rotor side, and then the stator side signal is measured. Rotor angle position and speed are estimated from the signals' phase shift and frequency. Its effectiveness and accuracy are influenced by the impedance value on the power grid side. An interesting approach is using frequency methods based on fast Fourier transform (FFT) analysis to identify and extract a spectral frequency in the generator's electrical signals that have a known relationship to rotor speed to estimate rotor position [22]. These algorithms require the use of fast digital signal processor (DSP) processors and are characterized by a decrease in estimation accuracy along with a decrease in the load on the generator system [23].

The next very interesting group is variable state observers based on the Luenberger theory and generator vector models. These advanced estimation algorithm solutions generally are divided into two groups, the full-order [24], [25] and reduced-order [26], [27], with different technic approaches. In [28] the full-order observer is proposed where the rotor position estimation error is regarded as an additional machine parameter, and it is tracked by the proposed adaptive law that makes compensation for the projection error from the rotor reference frame to the stator reference frame. A full-order observer is also shown in [29], [30], and [31], but the backstepping technique was used to improve performance. The most important task for the variable state observer is his stability in a wide range of machine rotor speeds both below and above the synchronous speed and variationist in generator parameters.

The main contribution of this article is to propose and extend the non-adaptive estimation scheme of position and the rotor speed of the DFIG system, which was first time proposed in [32]. The proposed observer is based on the DFIG mathematical model derived for the stator and rotor current vectors and stabilized using the Lyapunov method. The proposed solution brings benefits, in particular during the uncertainty of parameters of DFIG, disturbances in the measurement of the generator stator and rotor currents, and the generator operating states from the sub-and super-synchronous speed range. The order of observer structure is decreasing in comparison to adaptive structure, from $r = 6$ to $r = 5$. The problem with tuning the observer does not exist. The observer structure presented in [32] is extended to the stability analysis and uncertainties of chosen parameters. The simple adaptation mechanism is proposed to adjust the introduced in [32] tuning gain, which limits the overshoots of estimation errors during dynamic states of dynamic states the DFIG shown in Sections III and IV.

Presented simulation and experimental tests for a 2 kW generator show the state variables' small value of estimation errors and excellent performance in all working ranges.

II. Mathematical Model of Doubly-Fed Generator

The mathematical model of the DFIG system can be determined in different reference frames (stationary or rotating frames). The differential equations for the rotor and stator current vector components were presented in [9] and [30]

$$\frac{d\vec{i}_r}{d\tau} = -\left(\frac{L_s R_r}{w_\sigma} - j\omega_r \frac{L_s L_r}{w_\sigma}\right)\vec{i}_r + \left(\frac{L_m R_s}{w_\sigma} + j\omega_r \frac{L_s L_m}{w_\sigma}\right)\vec{i}_s + \frac{L_s}{w_\sigma}\vec{u}_r - \frac{L_m}{w_\sigma}\vec{u}_s \tag{1}$$

$$\frac{d\vec{i}_s}{d\tau} = -\left(\frac{L_r R_s}{w_\sigma} + j\omega_r \frac{L_m^2}{w_\sigma}\right)\vec{i}_s + \left(\frac{L_m R_r}{w_\sigma} - j\omega_r \frac{L_m L_r}{w_\sigma}\right)\vec{i}_r - \frac{L_m}{w_\sigma}\vec{u}_r + \frac{L_r}{w_\sigma}\vec{u}_s \tag{2}$$

and the electromechanical equation for the rotor angular speed

$$\frac{d\omega_r}{d\tau} = \frac{1}{J}(T_e - T_L - f_r\omega_r) \tag{3}$$

$$\frac{d\theta_r}{d\tau} = \omega_r \tag{4}$$

where

$$w_\sigma = L_r L_s - L_m^2$$

where $\vec{i}_s, \vec{i}_r, \vec{u}_r, \vec{u}_s$ are the currents and voltages of rotor and stator vectors, respectively, T_e and T_L are the electromagnetic and load torque, f_r is the coefficient of viscous friction. It is assumed that all machine parameters are known; the stator current vector components and the stator voltage vector components can be measured; the rotor voltage vector components are the control variables; rotor current vector components, as well as the rotor angular speed ω_r, are estimated by the speed observer structure. The generator is connected to the ac grid from the stator side and to the voltage source converter VSC from the rotor side.

III. Speed and Position Observer of DFIG

A. Speed Observer Structure and Stabilizing Functions

Considering the model (1)–(4) in (xy) rotating reference frame for $\omega_a = 0$ and coordinate changes within the IM model $f(i_{rx}, i_{ry}, i_{sx}, i_{sy}, \omega_r, \theta_r) \rightarrow f(i_{rx}, i_{ry}, H_x, H_y, \omega_r, \theta_r)$, the

following mathematical model of the machine is achieved

$$\frac{di_{rx}}{d\tau} = -\frac{L_s}{w_\sigma}(H_y + R_r i_{rx} + u_{rx}) + \frac{L_m}{w_\sigma}(R_s i_{sx} - u_{sx}) \quad (5)$$

$$\frac{di_{ry}}{d\tau} = \frac{L_s}{w_\sigma}(H_x - R_r i_{ry} + u_{ry}) + \frac{L_m}{w_\sigma}(R_s i_{sy} - u_{sy}) \quad (6)$$

$$\frac{dH_x}{d\tau} = \omega_r(-H_y - R_r i_{rx} + u_{rx}) + \frac{1}{\omega_r}\frac{d\omega_r}{d\tau}H_x \quad (7)$$

$$\frac{dH_y}{d\tau} = \omega_r(H_x - R_r i_{ry} + u_{ry}) + \frac{1}{\omega_r}\frac{d\omega_r}{d\tau}H_y \quad (8)$$

$$\frac{d\theta_r}{d\tau} = \omega_r + v_\theta \quad (9)$$

where

$$H_x = \omega_r\left(L_m i_{sx} + L_r i_{rx}\right) \quad (10)$$

$$H_y = \omega_r\left(L_m i_{sy} + L_r i_{ry}\right). \quad (11)$$

The speed observer structure is based on the mathematical model (5)–(9). The observer for this model has the following form:

$$\frac{d\hat{i}_{rx}}{d\tau} = -\frac{L_s}{w_\sigma}\left(\hat{H}_y + R_r i_{rx} + u_{rx}\right) + \frac{L_m}{w_\sigma}\left(R_s i_{sx} - u_{sx}\right) + v_{rx} \quad (12)$$

$$\frac{d\hat{i}_{ry}}{d\tau} = \frac{L_s}{w_\sigma}\left(\hat{H}_x - R_r i_{ry} + u_{ry}\right) + \frac{L_m}{w_\sigma}(R_s i_{sy} - u_{sy}) + v_{ry} \quad (13)$$

$$\frac{d\hat{H}_x}{d\tau} = \hat{\omega}_r\left(-\hat{H}_y - R_r i_{rx} + u_{rx}\right) + \hat{\omega}_r^{-1}\frac{d\hat{\omega}_r}{d\tau}\hat{H}_x + v_{Hx} \quad (14)$$

$$\frac{d\hat{H}_y}{d\tau} = \hat{\omega}_r\left(\hat{H}_x - R_r i_{ry} + u_{ry}\right) + \hat{\omega}_r^{-1}\frac{d\hat{\omega}_r}{d\tau}\hat{H}_y + v_{Hy} \quad (15)$$

$$\frac{d\hat{\theta}_r}{d\tau} = \hat{\omega}_r + v_\theta \quad (16)$$

where estimated state variables are marked by "^" and

$$\hat{H}_x = \hat{\omega}_r\left(L_m i_{sx} + L_r \hat{i}_{rx}\right) \quad (17)$$

$$\hat{H}_y = \hat{\omega}_r\left(L_m i_{sy} + L_r \hat{i}_{ry}\right). \quad (18)$$

The new input variables v_{rx}, v_{ry} and v_{Hx}, v_{Hy}, v_θ are introduced to the observer structure, which can be named as the stabilizing functions and allow the observer convergence to the real value of the machine. The stabilizing functions will be obtained by using the Lyapunov theorem. The estimation errors in the observer system can be defined as follows:

$$\tilde{i}_{rx} = \hat{i}_{rx} - i_{rx}, \tilde{i}_{ry} = \hat{i}_{ry} - i_{ry}, \tilde{H}_x = \hat{H}_x - H_x, \tilde{H}_y = \hat{H}_y - H_y, \tilde{\theta}_r = \hat{\theta}_r - \theta_r. \quad (19)$$

The rotor speed in the DFIG system depends on the wind speed of the turbine, which is assumed to be constant. Therefore, the derivative of the rotor speed, which occurs in (14) and (15) can be approximated, considering the time ΔT between calculating the rotor speed $d\hat{\omega}_r/d\tau \approx \Delta\hat{\omega}_r/\Delta T$. This simplification does not significantly influence the accuracy of the speed observer because the rotor speed is treated as the parameter whose value in the DFIG system is constant.

Considering the defined errors in (19) as well as (5)–(9) and (12)–(16) the model of estimation errors has the following form:

$$\frac{d\tilde{i}_{rx}}{d\tau} = -\frac{L_s}{w_\sigma}\tilde{H}_y + v_{rx} \quad (20)$$

$$\frac{d\tilde{i}_{ry}}{d\tau} = \frac{L_s}{w_\sigma}\tilde{H}_x + v_{ry} \quad (21)$$

$$\frac{d\tilde{H}_x}{d\tau} = \hat{\omega}_r(-\tilde{H}_y + R_r\tilde{i}_{rx}) + v_{Hx} \quad (22)$$

$$\frac{d\tilde{H}_y}{d\tau} = \hat{\omega}_r(\tilde{H}_x - R_r\tilde{i}_{ry}) + v_{Hy} \quad (23)$$

$$\frac{d\tilde{\theta}_r}{d\tau} = v_\theta \quad (24)$$

where in (20) and (21) the stator and rotor current components are treated as measured values [as the inputs to the observer system (12)–(16)].

The speed observer (12)–(16) will be asymptotically stable if the Lyapunov function is positively defined

$$V = \frac{1}{2}\left(\tilde{i}_{rx}^2 + \tilde{i}_{ry}^2 + \tilde{H}_x^2 + \tilde{H}_y^2 + \tilde{\theta}_r^2\right) > 0. \quad (25)$$

The derivatives of the function (25) by using (20)–(24) has the following form:

$$\dot{V} = -c_x\tilde{i}_{rx}^2 - c_y\tilde{i}_{ry}^2 + \tilde{i}_{rx}\left(c_x\tilde{i}_{rx} + v_{rx}\right) + \left(c_y\tilde{i}_{ry} + v_{ry}\right) + \tilde{H}_x\left(\hat{\omega}_r R_r\tilde{i}_{rx} + \frac{L_s}{w_\sigma}\tilde{i}_{ry} + v_{Hx}\right) + \tilde{H}_y\left(-\hat{\omega}_r R_r\tilde{i}_{ry} - \frac{L_s}{w_\sigma}\tilde{i}_{rx} + v_{Hy}\right) + \tilde{\theta}_r\left(v_\theta\right) \le 0. \quad (26)$$

The derivative of the Lyapunov function is negatively defined if the stabilizing functions are determined

$$v_{rx} = -c_x\tilde{i}_{rx} \quad (27)$$

$$v_{ry} = -c_y\tilde{i}_{ry} \quad (28)$$

$$v_{Hx} = c_{Hx}\left(-\frac{L_s}{w_\sigma}\tilde{i}_{ry} - \hat{\omega}_r R_r\tilde{i}_{rx}\right) \quad (29)$$

$$v_{Hy} = c_{Hy}\left(\frac{L_s}{w_\sigma}\tilde{i}_{rx} + \hat{\omega}_r R_r\tilde{i}_{ry}\right) \quad (30)$$

where $(c_x, c_y, c_{Hx}, c_{Hy}, c_\theta) > 0$ are the observer tuning gains.

B. Stability Analysis of the Observer System

Substituting (27), (28), (29), (30) to (26) for $(c_x, c_y, c_{Hx}, c_{Hy}, c_\theta) = 1.0$ is easy to check that the system is asymptotically stable

and the derivative of the Lyapunov function has the form

$$\dot{V} = -(\tilde{i}_{rx}^2 + \tilde{i}_{ry}^2 + c_\theta \tilde{\theta}_r^2) \le 0, c_\theta > 0. \tag{31}$$

Assuming the ideal condition, it can be considered that $c_x = c_y = c_{xy}$ and $c_{Hx} = c_{Hy} = c_H$ and the minimum values of these tuning gains should be at least

$$c_{xy} > 1 \text{ and } c_H > \sqrt{\left(\hat{\omega}_r R_r \tilde{i}_{rx} + \frac{L_s}{w_\sigma}\tilde{i}_{ry}\right)^2 + \left(\hat{\omega}_r R_r \tilde{i}_{ry} + \frac{L_s}{w_\sigma}\tilde{i}_{rx}\right)^2}. \tag{32}$$

To satisfy the Lyapunov theorem $\dot{V} < 0$, the stabilizing function v_θ should be

$$v_\theta = -c_\theta \tilde{\theta}_r. \tag{33}$$

In the sensorless control, the rotor speed is not measured; therefore, the deviation $\tilde{\theta}_r$ in (33) should be replaced by $\tilde{\theta}_H$, which means the difference between the estimated values of H_x and H_y, calculated from (17) and (18) and reconstructed from the observer structure by using (14) and (15) as follows [30]:

$$\tilde{\theta}_H = \tan^{-1}(\vartheta) \tag{34}$$

$$\text{where } \vartheta = \frac{H_x \hat{H}_y - H_y \hat{H}_x}{H_x \hat{H}_x + H_y \hat{H}_y} \text{ and } (H_x \hat{H}_x + H_y \hat{H}_y) \neq 0. \tag{35}$$

Then, since the system (5)–(9) stays in operation domain D, hence if

$$c_x = \max\{\tilde{i}_{rx}\} + \delta_1 \tag{36}$$

$$c_y = \max\{\tilde{i}_{ry}\} + \delta_2 \tag{37}$$

$$c_\theta = \max\left\{\tilde{\theta}_r \omega_r^{-1}\right\} + \delta_\theta \tag{38}$$

with δ_1, δ_2, $\delta_\theta > 0$ and for $\tilde{i}_{rx,y} \le \varepsilon_1$, $\tilde{\theta}_r \le \varepsilon_2$, $\tilde{\omega}_r \le \varepsilon_3$ and $\varepsilon_{1,2,3} << 1$ are sufficient small reals, the derivative of the Lyapunov function takes the following form:

$$\dot{V} = -\delta_1 |\tilde{i}_{rx}| - \delta_2 |\tilde{i}_{ry}| - \delta_\theta |\tilde{\theta}_r| \le -\mu\sqrt{V} \tag{39}$$

where $\mu = \min(\sqrt{2}\delta_3, \sqrt{2}\delta_\theta)$ and $\delta_3 = \delta_1 + \delta_2$.

The condition (39) implies the convergence of vector values $\hat{\boldsymbol{i}}_r$ to $\boldsymbol{i}_r$ and $\vec{\boldsymbol{H}}$ to $\boldsymbol{H}$, hence $\hat{\theta}_r$ tend to real value θ_r in finite time, noted as t_2.

Remark 1: The rotor speed value can be determined from the following dependence [32]

$$\hat{\omega}_r = \frac{\hat{H}_x \hat{\psi}_{rx} + \hat{H}_y \hat{\psi}_{ry} - c_f s_\omega}{\hat{\psi}_{rx}^2 + \hat{\psi}_{ry}^2} \tag{40}$$

$$s_\omega = \hat{H}_x \hat{\psi}_{ry} - \hat{H}_y \hat{\psi}_{rx} \tag{41}$$

where

$$\hat{\psi}_{rx} = L_m i_{sx} + L_r \hat{i}_{rx} \tag{42}$$

$$\hat{\psi}_{ry} = L_m i_{sy} + L_r \hat{i}_{ry} \tag{43}$$

are the rotor flux components that can be calculated from the above dependencies.

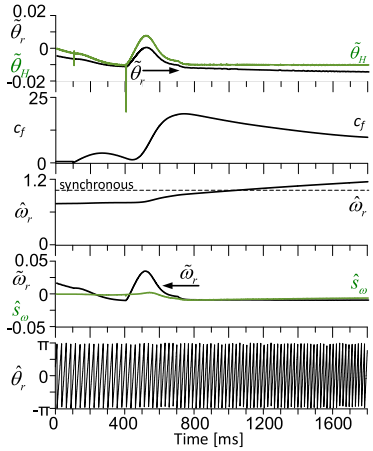

Fig. 1. DFIG is crossing from subsynchronous to supersynchronous speed, after 100 ms the value of c_f is determined from (44). Simulation results.

It is worth noticing that if (39) is satisfied, then the vectors of estimated values tend to their real in finite time, noted as t_2 and $\hat{\psi}_{rx}^2 + \hat{\psi}_{ry}^2 \neq 0$ the rotor flux vector components defined in (42) and (43), tend to real values in finite time, noted as t_3, and the same the rotor speed estimated from (40), converges exponentially to its real value ω_r. For (c_x, c_y, c_{Hx}, c_{Hy}, c_θ, c_f) > 0, the observer system is practically stable [33].

Remark 2: The form of (40) results from (17) and (18) by using (42) and (43). The value of s_ω defined in (41) depends on the mutual position of the vectors $\vec{\boldsymbol{H}}$ and $\vec{\boldsymbol{\psi}}_r$. For the perpendicular case, the $s_\omega = 0$ because $s_\omega = \cos(\vec{\boldsymbol{H}}, \vec{\boldsymbol{\psi}})$ this is the scalar product of the vectors. In the rotor speed dependence, (40) the value of c_f can be determined by using a simple adaptation mechanism

$$\frac{dc_f}{d\tau} = \gamma \text{sgn}(s_{\omega f})(s_{\omega ref} - s_{\omega f}) \tag{44}$$

where $s_{\omega f}$ means the filtrated signal of s_ω by using LPF with $1/T = 0.005$ and $s_{\omega \text{ref}}$ is the reference value of the scalar product, which in the ideal condition could be equal to zero and it is assumed $\gamma = 10/T = 0.05$ p.u.

In Fig. 1, in the DFIG system, the active reference power is set to -0.1 p.u. and reactive power -0.6 p.u. The rotor speed crosses from the sub to the supersynchronous range. The value of c_f coefficient is estimated from (44) and limited according to (45). For the subsynchronous speed range, the cf value is about 1.0 up to 3 (depending on the generator load). If the rotor speed is increased, the value of c_f is not constant, and during the dynamic state is about $c_f = 20$ p.u. After that, it settles to about 10–11 p.u. The same behavior is visible in the experimental tests.

The maximum value of c_f for $(\hat{\psi}_{rx}^2 + \hat{\psi}_{ry}^2) \approx 1$, $|\hat{\omega}_{r\max}| = 1.2$ p.u. and $|s_{\omega ref}| = 0.005$ can be determined

$$c_{f\max} = \frac{\hat{H}_x \hat{\psi}_{ry} - \hat{H}_y \hat{\psi}_{rx} + |\hat{\omega}_{r\max}|}{|s_{\omega ref}|} \tag{45}$$

and c_f should be chosen $0 \le c_f \le c_{f\max}$. The observer scheme with the folwchart diagram is presented in Fig. 2.

Remark 3: As aforementioned, the observer structure will be stable for the tuning gains determined from (32) and (38). The

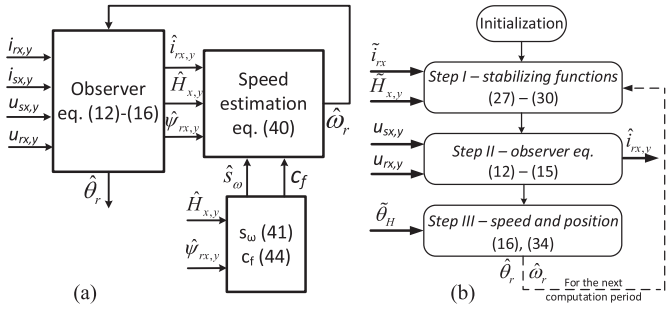

Fig. 2. (a) Scheme of the observer structure. (b) Flowchart diagram for the observer structure.

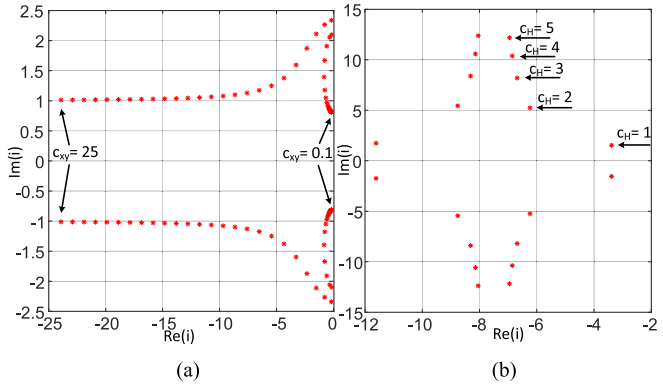

Fig. 3. Spectrum of matrix **A** of the linearized observer system for $\omega_r = 0.8$ p.u. and a) $c_\theta = 0$, b) $c_{xy} = 15$, $c_\theta = 0.1$ p.u.

observer tuning gains influence the speed of observer convergences. It is worth noticing that for $c_\theta = 0$, the observer structure is unstable due to the open integrator (16). The tuning gains can be specified from the model of observer errors linearized near an equilibrium point in the (d–q) reference frame connected to the stator flux vector. The general form of the linearized system is

$$\frac{d}{dt}\Delta \mathrm{x}(t) = \mathrm{A}\Delta \mathrm{x}(t) + \mathrm{B}\Delta \mathrm{u}(t) \tag{46}$$

where **A** and **B** are the Jacobian matrices; $\Delta \mathrm{x}(t) = [\tilde{i}_{rd}, \tilde{i}_{rq}, \tilde{H}_x, \tilde{H}_y, \tilde{\theta}_r]^T$; $\Delta \mathrm{u}(t)$ is treated as known control inputs.

By using the observer errors model (20), (21), (22), (23) and for (dq), the matrix **A** can be determined as follows:

$$\boldsymbol{A} = \begin{bmatrix} -c_{xy} & \omega_\psi & 0 & -a_1 \\ -\omega_\psi & -c_{xy} & a_1 & 0 \\ \omega_r^* R_r(1-c_H) & -c_H a_1 & 0 & -\omega_r^* \\ c_H a_1 & -\omega_r^* R_r(1-c_H) & \omega_r^* & 0 \end{bmatrix} \tag{47}$$

where $a_1 = L_s/w_\sigma$ and values of ω_r^* are determined for the chosen working points and $\omega_\psi = 1.0$ p.u.

It is worth noticing that the position error equation is omitted in the linearized system because the rotor speed is treated as the parameters, and due to the open integrator form, the value of c_θ should always be $c_\theta \neq 0$. For $c_\theta = 0$, it is easy to check that the one pole of the system matrix $\boldsymbol{A}$ has equal to zero. It means that the observer system has undamped oscillations. Therefore, it can be assumed that $c_\theta \neq 0$ and to analyze the reduced linearized system order with $n = 4$. The spectrum of the matrix of the linearized observer system for different tuning gains value c_{xy} from 0.1 to 25 is presented in Fig. 3(a). The values of poles are close to zero for $c_\theta = 0$. In Fig. 3(b) the value of c_H is changed from 1 to 5 p.u., but $c_\theta = 0.1$ p.u.

The next section confirms the theoretical investigations by using the simulation results in the 2 kW DFIG system.

IV. Simulation Results

The simulation model of the DFIG system contains the doubly-fed machine model, wind emulators, and the VSI model with the space vector modulation (SVM).

The sample period for the control system is 150 μs and for the SVM is 300 μs. The system parameters are given in Table II.

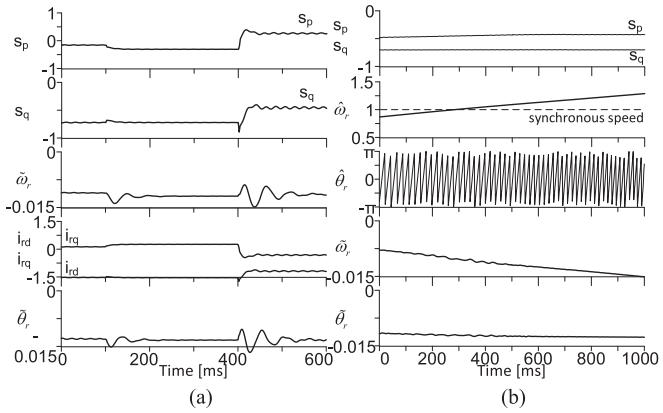

Fig. 4. (a) Active and reactive power changes for the constant rotor speed of about 0.8 p.u. (b) Crossing from subsynchronous to supersynchronous rotor speed from 0.72 to 1.25 p.u.

In Fig. 4(a) the active power (s_p) is changed from -0.1 to -0.35 after 100 ms (reactive power (s_q) is set to -0.6), and after 400 ms, the active and reactive powers are changed together - s_p to 0.35, s_q to 0.2 p.u. As a result, the estimation error of rotor speed is smaller than 0.01 in the steady-state and about 0.015 in the transient state. On the other hand, the rotor position error is about 0.012 in the steady state and approximately 0.017 in the transient state. The components of rotor current i_{rd}, i_{rq} are shown.

In Fig. 4(b) the active power s_p is set to 0.02 p.u. and reactive power s_q is set to -0.6 p.u. The rotor speed of the DFIG is changed from the subsynchronous to supersynchronous mode. The estimated speed error is increased during the rotor speed crossing through the synchronous speed (1.0 p.u.). The error of rotor position is almost constant and at about 0.01 p.u.

In Fig. 5(a) the rotor current estimation errors $\tilde{i}_{rx,yS}$, rotor flux "x" component ψ_{rxS}, measured and estimated rotor position, estimated rotor speed and rotor speed and position errors, and rotor current vector components for the DFIG steady-state are presented. The rotor speed and position errors are about 0.015 p.u. In Fig. 5(b) the DFIG parameters uncertainties test is presented. After 300 ms the stator resistance is changed twice. The rotor position error is changed from -0.012 to 0.012 rad; the

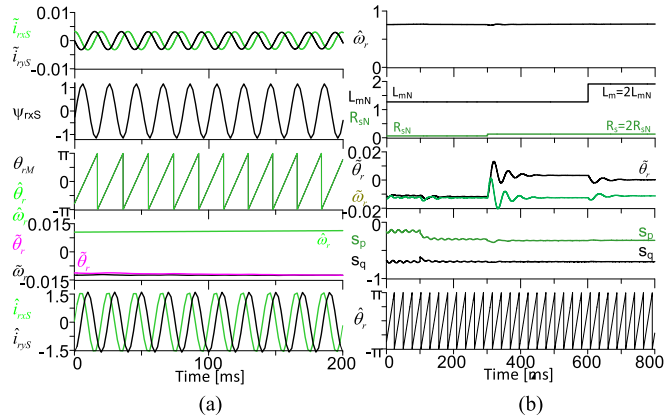

Fig. 5. (a) Steady-state of DFIG and the estimated variables by the speed observer and their errors for subsynchronous mode – index "S" means reference frame connected to the stator. (b) After 300 ms the stator resistance and after 600 ms magnetizing inductance are changed twice.

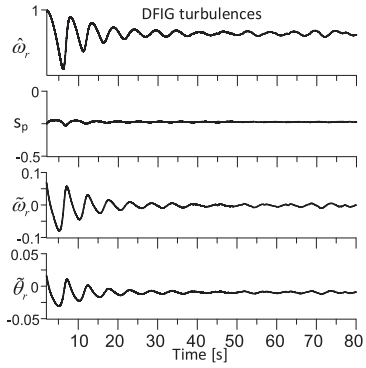

Fig. 6. Turbulences in DFIG system are modelled.

rotor speed error is below 0.01 p.u. in the stationary state; after 600 ms, the nominal value of magnetizing inductance is twice (together with stator and rotor inductance). This change has resulted in a reduction of the errors of rotor speed and position below 0.01. Changes in the nominal value of stator resistance and the magnetizing inductance do not affect the stability of the proposed observer structure.

In Fig. 6, the DFIG turbulences are modeled. The turbulences are turned on in the control system. It is visible that the estimated rotor speed has oscillated; however, the estimated speed and position errors are below 0.02. in the steady state. The proposed observer is stable during these simulated conditions.

The theoretical issues are confirmed using experimental investigations presented in the following section.

V. Experimental Results

Experimental results were carried out in the 2 kW generator system (Table II in Appendix). The sensorless control system with the Field-oriented control from Fig. 5 was implemented in a DSP board with a Sharc ADSP21363 floating-point signal processor and Altera Cyclone II FPGA. The PWM switching frequency was 3.3 kHz. The code of the algorithm was not

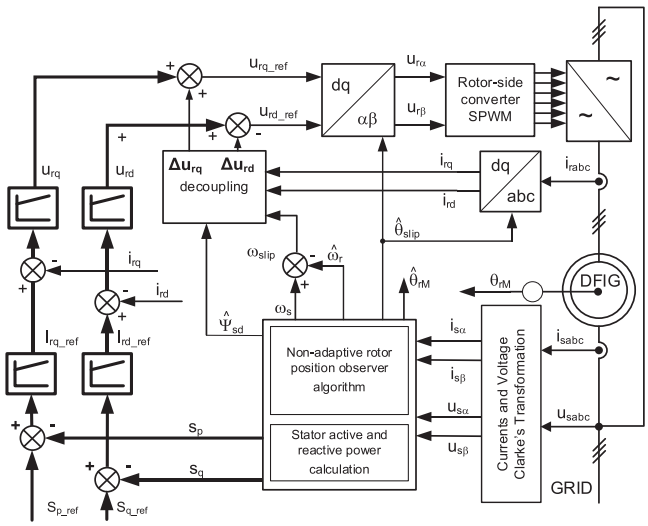

Fig. 7. Vector control structure for the rotor side converter.

optimized for a DSP processor. The interruption time was set at 150 μs. The sensorless control system structure is shown in Fig. 7. The experimental stand contains the DFM connected to the squire cage induction machine. The stator of DFM was supplied to the ac grid. The rotor was connected to the ac grid through the voltage source converter. The computing time of the proposed sensorless control system structure is 42 μs. The observer structure tuning gains are chosen using stability analysis of the observer presented in Section III: $c_{x,y} = 10$, $c_{Hx,y} = 2$, $c_\theta = 0.1$ p.u., $c_f = 5 \ldots 15$ [or using the adaptive (44)].

The experimental investigations are divided into the following scenarios: steady-state of the DFIG, nominal power changes of active and reactive, and nominal parameters uncertainties. In the figures, the selected variables are presented as follows.

1) s_p, s_q active and reactive power respectively.
2) $\hat{\omega}_r$ estimated rotor speed and their error $\tilde{\omega}_r$.
3) Estimated $\hat{\theta}_r$ and measured θ_{rM} value of the rotor position and their error $\tilde{\theta}_r$.
4) Values of the signals s_ω and $\hat{\theta}_H$.
5) Stator and rotor vector components i_{sxS}, $\hat{i}_{rx,yS}$.
6) Error of the estimated rotor vector component $\tilde{i}_{rxS}$.
7) Rotor flux vector components $\hat{\psi}_{rx,yS}$.

A. Steady State of the DFIG System

In this scenario, the DFIG is in the steady state in which the active power is set to -0.1 p.u. and reactive power is set to -0.6 p.u. the rotor speed is about 0.72 p.u. In Fig. 8(a) the estimated rotor speed, rotor current vector components $\hat{i}_{rx,yS}$, and rotor flux vector components $\hat{\psi}_{rx,yS}$ are shown. The current vector components have visible higher harmonics resulting from the machine's design (slots harmonics [30]). In Fig. 8(b), the rotor speed is about 0.82 p.u. and the measured and estimated rotor position, stator vector component i_{sxS}, and the error of the estimated rotor vector component $\tilde{i}_{rxS}$ are shown. The average value of error $\tilde{i}_{rxS}$ is smaller than 0.02 p.u.

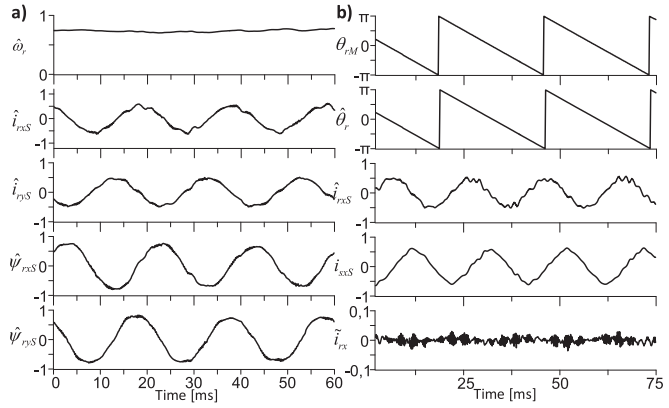

Fig. 8. Steady-state of the DFIG system, selected variables are presented.

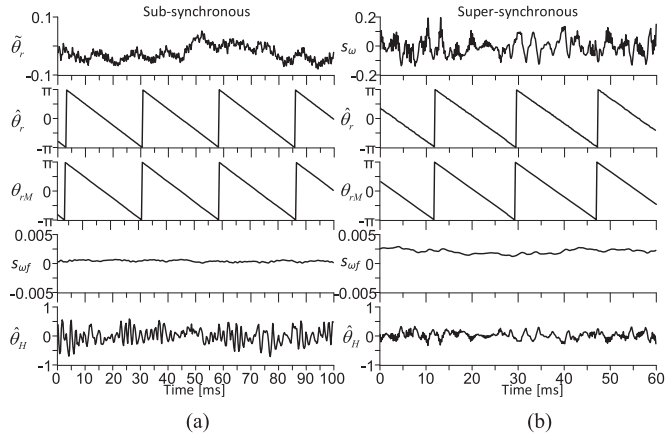

Fig. 9. Steady-state for (a) subsynchronous speed range ($\omega_r = 0.75$ p.u.) and (b) supersynchronous speed range ($\omega_r \sim 1.2$ p.u.).

In Fig. 9(a) the chosen variables in the steady state of the DFIG are presented. For the subsynchronous range, the rotation speed is about 0.75 p.u. for the supersynchronous range, which is about 1.2 p.u. The estimated and measured rotor position values are compared, and the values of filtrated scalar product $s_{\omega f}$ and stabilizing function $\tilde{\theta}_H$ are shown. In Fig. 9(a) the value of $s_{\omega f}$ is almost equal to zero, and the value of c_f is determined using the adaptive term (44) for $s_{\omega ref} = 0.001$ p.u. The estimation of position error is then about -0.03 rad.

In the supersynchronous case presented in Fig. 9(b), the value of $s_{\omega \mathrm{ref}} = 0.001$ p.u. However, $s_{\omega f} \sim 0.0025$ p.u. and the value of c_f is limited to $c_{f\max} = 20$ [from(45)]. Respectively, the generator's active power was set to -0.3 p.u. and reactive to -0.4 p.u.. The filtrated value of $s_{\omega f}$, as well as instantaneous s_{ω}, are presented.

B. Dynamic States of DFIG

In Fig. 10(a) the active power is changed to -0.35 p.u., and reactive power is maintained to a constant value of -0.6 p.u. The estimated rotor speed error in the transient state is 0.05 p.u. in the steady state is smaller than 0.02 p.u. The estimated rotor

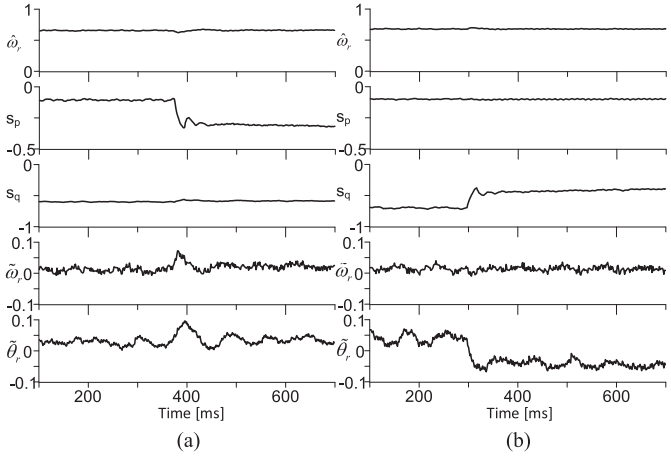

Fig. 10. (a) Reactive power is equal to -0.6 p.u. and after 400 ms, the active power is changed to -0.35 p.u. (b) Active power is -0.1 p.u. and after 300 ms, the reactive power is changed to -0.4 p.u.

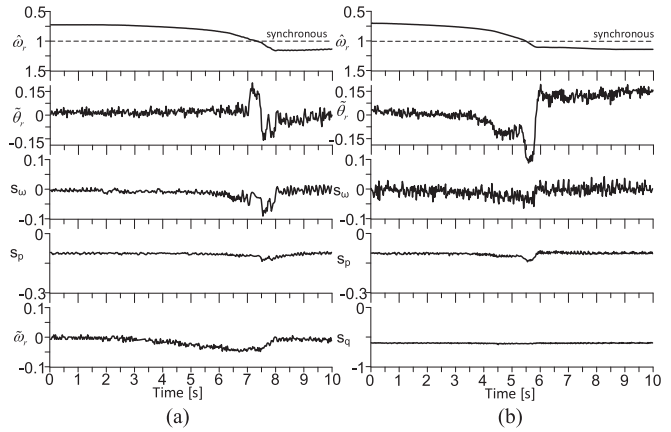

Fig. 11. Characteristic speed observer waveforms for the crossing of generator rotor speed through synchronous speed for (a) value of c_f is determined adaptively from (44), and (b) $c_f = 11$ and it is constant.

position error is about 0.1 rad. in the transient state and, after this, is decreased to about 0.04 p.u. In Fig. 10(b), after 300 ms, the reactive power is changed from -0.6 to -0.4 p.u. The rotor speed error is constant and at about 0.02 p.u. however, the rotor position error is increased to 0.07 rad. This error occurs after the value of the reactive power is decreased to -0.4 p.u. This test confirms that the reactive power value influences the estimation errors of the speed observer structure.

In Fig. 11 the rotation speed of the generator rotor increases from 0.72 to 1.25 p.u. as a result of increasing the external driving torque of the generator. The generator power control system works correctly, the values of active and reactive power set in the control system are kept almost constant around reference values. The time waveforms presented in Fig. 11 refer to the unfavorable operating point with an underloaded generator. The references to active and reactive powers are -0.1 and -0.6 p.u., respectively. The sensorless control system works stable, crossing through the synchronous rotor speed. The rotor position error is smaller than 0.15 rad. in the transient states and, after reaching the

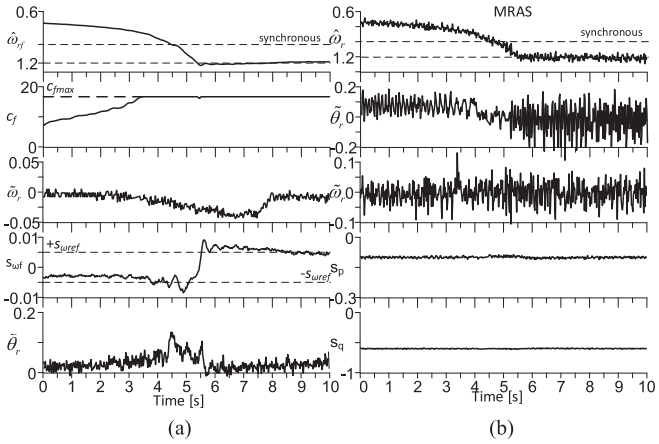

Fig. 12. DFIG is crossing from subsynchronous to supersynchronous speed; the value of c_f is determined from (44).

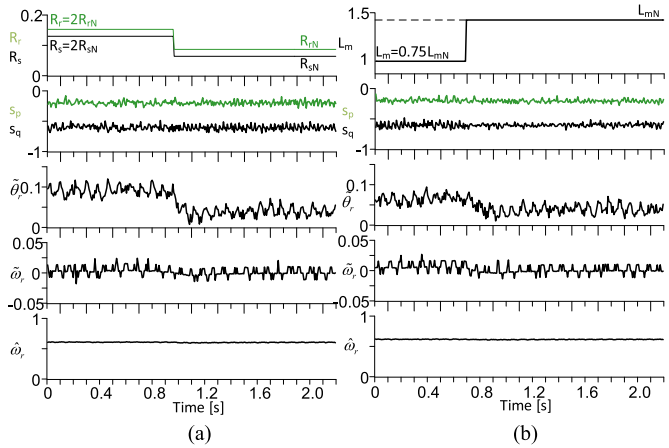

Fig. 13. Uncertainties of nominal parameters in the speed observer structure for (a) after 0 s $R_{s,r} = 2R_{s,rN}$ and after 1 s, $R_{s,r} = R_{s,rN}$, (b) after 0 s $L_m = 0.75L_{mN}$ and after 0.8 s $L_m = L_{mN}$.

synchronous speed, is decayed to the constant of about -0.05 p.u. The value is maintained, and it results from $c_{f\max}$ and s_ω. It means that the vectors $\vec{\boldsymbol{H}}\ \vec{\psi}_r$ are not perpendicular $s_\omega \neq 0$. Hence, to minimize the position error, the value of c_f should not be limited to $c_{f\max}$. On the other hand, the term $(-c_f s_\omega)$ is introduced to (40) and without its bounded; the rotor speed value may not tend to the actual value though this $\hat{\theta}_r$ does not tend to real value θ_r in finite time, noted as $t_{2,}$ and the observer system can be unstable.

In Fig. 11(b), the value of c_f is set to constant value $c_f = 11$ p.u. The constant value of c_f was presented in [32]. For this case, the maximum value of the estimated error of rotor position is about 0.15 rad in the supersynchronous speed range. The sensorless control system is stable. In Fig. 12, the DFIG crosses from $\omega_r = 0.75$ to $\omega_r = 1.2$ p.u. The cf value is estimated adaptively using (44) and bounded to $c_{f\max}$. Then the value of s_ω is changed from $-s_\omega$ to $+s_{\omega,}$ which is visible in Fig. 12. Therefore $\mathrm{sgn}(s_{\omega f})$ is added to (44). The estimation error of the rotor position during the transient state is about 0.12 p.u.; however, in the steady state is smaller than 0.05 p.u. In Fig. 12(b) the chosen variables are presented for the MRAS observer presented in [34]. The active power is set to -0.1 and the reactive power to -0.6 p.u. The MRAS system is stable; however, the estimated position and speed oscillate. The average rotor position is about 0.12 [rad].

The coefficient c_f in (40) has not a physical meaning. However, this value influences the estimated rotor speed and position. This minimizes the position and rotor speed errors, particularly in the crossing through the synchronous speed visible in Fig. 12.

C. Parameter Uncertainties of DFIG

The uncertainties test of the parameters in the observer system was carried out to check the behavior of the proposed observer to the variability of chosen nominal parameters. The values of the stator and rotor resistances are changed at the same time. These values were changed two times according to $R_{s,r} = 2R_{s,rN}$. This test is presented in Fig. 13(a). The active and reactive powers are -0.1 and -0.6 p.u., respectively. The rotor speed is about 0.75 p.u. After 0 s values of the resistances are changed, and after 1s, the nominal values are set. The estimated value of rotor position error is about 0.1 rad. In Fig. 13(b), after 0 s nominal value of the magnetizing inductance $L_m = 0.75L_{mN}$, and after 0.8 s is set to the nominal value. The estimated rotor position error is about 0.07 rad. Changes in the nominal parameters of the generator do not stimulate the observer structure significantly and have the influence of a negative effect on the estimated rotor position value, however, for the assumed range of the parameters changes, the observer structure is stable.

VI. Discussion

The performance of the proposed non-adaptive speed estimation approach is shown in Sections IV and V. The proposed sensorless control system works stable even if the nominal parameters of the generator are changed. This test has been presented in Fig. 13. The error of rotor position is increased up to 0.1 rad; for the nominal parameters is decreased up to 0.04 p.u. (for $R_{s,r} = 2R_{s,rN}$); almost the same position error value occurs during the changes of the nominal value of the magnetizing inductance $L_m = 0.75L_{mN}$ [see Fig. 13(b)]. The average error of estimated rotor speed is always below 0.025 p.u.; and higher in case of uncertainties of L_m. In Fig. 10 the responses of the stator's active and reactive power are shown. As shown in Fig. 10(b), the observer structure is sensitive to reactive power changes. In this case, the estimated position errors changed their value from positive to negative; however, their average value does not change and is kept to about 0.05 rad. In Figs. 11 and 12 the rotor speed of DFIG is changed from subsynchronous to supersynchronous. The rotor speed is estimated non-adaptively; however, the additional stabilizing function is introduced to the estimation law (40) and particularly described in Section III. The reinforcement of this function marked as c_f can be determined as the constant or by an adaptive approach (44). Both cases are shown in Fig. 11. After changing the rotor speed, for $c_f = 11$ [see Fig. 11(b)], the estimated rotor position has a constant value of about 0.15 p.u. While c_f is adaptively estimated, the position

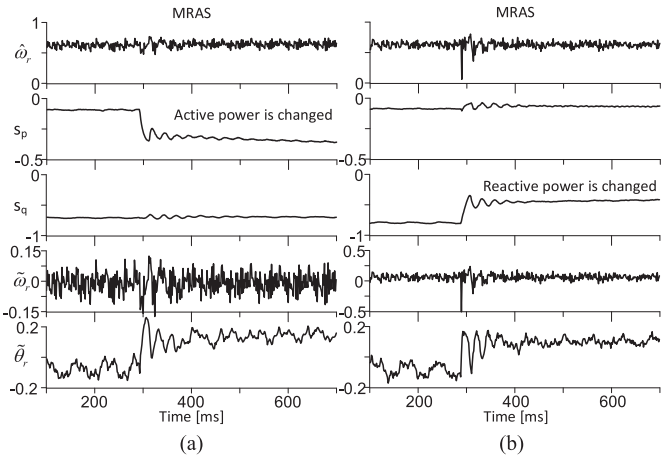

Fig. 14. MRAS [34](a) reactive power is equal to −0.6 p.u. and after 350 ms, the active power is changed to −0.35 p.u. and (b) the active power is −0.1 p.u. and after 300 ms the reactive power is changed to −0.4 p.u.

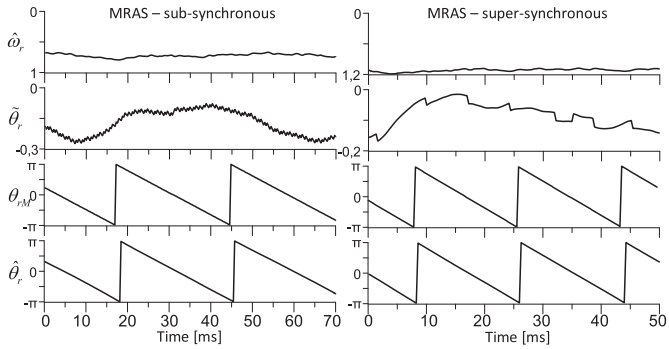

Fig. 15. MRAS [34], $s_p = -0.1$, $s_q = -0.7$ p.u. for (a) subsynchronous operation, and (b) supersynchronous operation, θ_{rM} is measured position.

error is minimized almost to 0.03−0.05 p.u., which is visible in Fig. 12(a).

The performance of the proposed observer structure was compared to the well-known [34] SFMO—MRAS structure. In the MRAS [34], the reinforcement in the integration part of PI controllers was taken 0.9 p.u.; for the error, the part was 1.0 p.u. The active power changes are shown in Fig. 14(a), while changes in the reactive power are in Fig. 14(b). The rotor position error is more oscillating than in the proposed observer structure. Their average value is above 0.18 rad [see Fig. 14(a)]. If the reactive stator power is generated after 300 ms, the power is −0.4 p.u., then the average rotor position error is 0.15 p.u. and their value is smaller than in Fig. 14(a). The rotor speed error is smaller than 0.05 p.u. for both cases.

Fig. 15 shows the estimated and measured rotor position waveforms and their error for subsynchronous and subsynchronous operation. The position error for the subsynchronous speed has a higher value (up to 0.27 rad) than the supersynchronous (up to 0.2 rad). In Fig. 12(b), the rotor speed is changed from the subsynchronous to supersynchronous operation for

TABLE I
SPEED AND POSITION ESTIMATION ERRORS

Observer structure	Proposed observer		MRAS [34]	
Test	I – changes of active and reactive powers	II – sub synchronous to super synchronous	I – changes of active and reactive powers	II – sub synchronous to super synchronous
Avg. speed estimation error [p.u.]	0.0135	-0.0133	0.0092	0.011
Avg. speed deviation [p.u.]	0.0063	0.018	0.0192	0.021
Avg. position estimation error [rad]	0.0137	0.0613	0.134	0.0506
Avg. position deviation [rad]	0.0502	0.0327	0.0496	0.045

Test:
I – changes of active and reactive powers.
II – from subsynchronous to supersynchronous of DFIG operation.

MRAS. It is visible that the rotor position error is changed from −0.15 to −0.2 rad during the changing of rotor speed. As a result, the maximum estimated rotor speed error has a value up to 0.07 p.u.

The comparison of estimation rotor speed and position errors between the proposed non-adaptive speed estimation structure and SFM—MRAS [34] is given in Table I.

VII. CONCLUSION

In the article, the speed and position observer structure which was based on the non-adaptive approach was considered. The non-adaptive dependence (40) was based on the scalar and cross-product of the introduced internal vector $\vec{\boldsymbol{H}}$ and the rotor flux vector $\tilde{\psi}_r$. The scalar product s_ω of the two vectors has not a constant value. However, its value depends on the DFIG working points (as mentioned in Section III-B and confirmed by simulation and experimental results). The integration of the estimated rotor speed value determines the rotor position. However, integrating the rotor speed value, especially for an initial condition, introduces the estimation error of the position. Therefore, it was proposed to introduce the stabilizing function to the position differential equation. This stabilizing function was based on the error angle between the estimated value of the vector $\vec{\boldsymbol{H}}$ and vector $\tilde{\psi}_r$ (calculated from measured values) multiplied by $\hat{\omega}_r$. It prevents the unstable of the whole observer structure and improves the properties, especially during the "difficult" DFIG working condition while the generator is crossing through the synchronous rotor speed (in which the frequency of the rotor current vector is close to zero).

The stabilizing functions in the proposed observer structure are determined using the Lyapunov approach. Based on the Lyapunov stability theorem of the linearized observer close to the equilibrium points and by the pole placement method, the

observer functions and introduced tuning gains are determined. The simulation and experimental results demonstrate the desired sensorless control system performance for a wide operating range. The proposed solution is characterized by "good" accuracy estimation for rotor position and speed. The accuracy of speed estimation does not exceed the value of 0.025 p.u. (2.5%) synchronous speed and 0.05 [rad] of rotor position in steady-state conditions. The observer structure is stable in the operating speed range demonstrated by laboratory tests.

Appendix

The DFIG nominal parameters are given in Table II. The drive system consists of a 4 kW squire-cage motor driving a 2 kW doubly-fed generator and an incremental encoder with a 720 pulse resolution to compare the results.

TABLE II
Generator Parameters and Reference Unit

Symbol	Quantity	Values
R_{sN}	stator resistance	2.833 Ω/ 0.067 p.u.
R_{rN}	rotor resistance	2.867 Ω/ 0.068 p.u.
L_{mN}	magnetizing inductance	0.15 H/ 1.123 p.u.
L_{sN}, L_{rN}	stator and rotor inductance	0.164 H/ 1.1227 p.u
L_σ	leakage inductance	0.014 H/
P_n	nominal power	2 kW
I_{ns}	nominal stator current	5.5 A
I_{nr}	nominal rotor current	3.4 A
U_n	nominal stator voltage	400 V
N	nominal rotor speed	910 rpm
f_n	nominal frequency	50 Hz
r	Turn ratio N_s/N_r	1
$U_b=U_n$	reference voltage	400 V
$I_b=\sqrt{3}I_{ns}$	reference current	9.52 A
S_b	reference power	3810 VA

References

[1] G. D. Marques and D. M. Sousa, "Stator flux active damping methods for field-oriented doubly fed induction generator," *IEEE Trans. Energy Convers.*, vol. 27, no. 3, pp. 799–806, Sep. 2012, doi: 10.1109/TEC.2012.2204887.

[2] R. M. Prasad and M. A. Mulla, "Mathematical modeling and position-sensorless algorithm for stator-side field-oriented control of rotor-tied DFIG in rotor flux reference frame," *IEEE Trans. Energy Convers.*, vol. 35, no. 2, pp. 631–639, Jun. 2020, doi: 10.1109/TEC.2019.2956255.

[3] R. M. Prasad and M. A. Mulla, "A novel position-sensorless algorithm for field-oriented control of DFIG with reduced current sensors," *IEEE Trans. Sustain. Energy*, vol. 10, no. 3, pp. 1098–1108, Jul. 2019, doi: 10.1109/TSTE.2018.2860993.

[4] L. Xu and P. Cartwright, "Direct active and reactive power control of DFIG for wind energy generation," *IEEE Trans. Energy Convers.*, vol. 21, no. 3, pp. 750–758, Sep. 2006, doi: 10.1109/TEC.2006.875472.

[5] S. Odhano, S. Rubino, M. Tang, P. Zanchetta, and R. Bojoi, "Stator current-sensorless-modulated model predictive direct power control of a DFIM with magnetizing characteristic identification," *IEEE J. Emerg. Sel. Topics Power Electron.*, vol. 9, no. 3, pp. 2797–2806, Jun. 2021, doi: 10.1109/JESTPE.2020.3024679.

[6] S. Mondal and D. Kastha, "Improved direct torque and reactive power control of a matrix-converter-fed grid-connected doubly fed induction generator," *IEEE Trans. Ind. Elect.*, vol. 62, no. 12, pp. 7590–7598, Dec. 2015, doi: 10.1109/TIE.2015.2459056.

[7] R. Patel, F. Hafiz, A. Swain, and A. Ukil, "Nonlinear rotor side converter control of DFIG based wind energy system," *Elect. Power Syst. Res.*, vol. 198, 2021, Art. no. 107358.

[8] J. Han, Z. Liu, and N. Liang, "Nonlinear adaptive robust control strategy of doubly fed induction generator based on virtual synchronous generator," *IEEE Access*, vol. 8, pp. 159887–159896, 2020, doi: 10.1109/ACCESS.2020.2994094.

[9] Z. Krzeminski, "Sensorless multiscalar control of double fed machine for wind power generators," in *Proc. Power Convers. Conf.-Osaka*, 2002, vol. 1, pp. 334–339.

[10] G. D. Marques and D. M. Sousa, "Sensorless direct slip position estimator of a DFIM based on the air gap *pq* vector-sensitivity study," *IEEE Trans. Ind. Electron.*, vol. 60, no. 6, pp. 2442–2450, Jun. 2013.

[11] G. D. Marques and D. M. Sousa, "New sensorless rotor position estimator of a 9DFIG based on torque calculations-stability study," *IEEE Trans. Energy Convers.*, vol. 27, no. 1, pp. 196–203, Mar. 2012.

[12] P. K. Gayen, "Stator flux producing current-based promoted rotor angle estimator of doubly-fed induction generator for encoderless operations," *IEEE Sensors J.*, vol. 21, no. 13, pp. 15133–15141, Jul. 2021, doi: 10.1109/JSEN.2021.3072396.

[13] P. K. Gayen, "An enhanced rotor position/speed estimation technique for doubly fed induction generator using stator-side reactive current variable in model reference adaptive system," *IEEE Trans. Ind. Electron.*, vol. 69, no. 5, pp. 4409–4418, May 2022, doi: 10.1109/TIE.2021.3086728.

[14] L.-Y. Lu, N. F. Avila, C.-C. Chu, and T.-W. Yeh, "Model reference adaptive back-electromotive-force estimators for sensorless control of grid-connected DFIGs," *IEEE Trans. Ind. Appl.*, vol. 54, no. 2, pp. 1701–1711, Mar./Apr. 2018, doi: 10.1109/TIA.2017.2765300.

[15] T. Nguyen and D.-C. Lee, "Sensorless control of DFIG wind turbine systems based on SOGI and rotor position correction," *IEEE Trans. Power Electron.*, vol. 36, no. 5, pp. 5486–5495, May 2021, doi: 10.1109/TPEL.2020.3027888.

[16] N. D. Dao, D. Lee, and S. Lee, "A simple and robust sensorless control based on stator current vector for PMSG wind power systems," *IEEE Access*, vol. 7, pp. 8070–8080, 2019.

[17] R. Zhao, Z. Xin, P. C. Loh, and F. Blaabjerg, "A novel flux estimator based on multiple second-order generalized integrators and frequency-locked loop for induction motor drives," *IEEE Trans. Power Electron.*, vol. 32, no. 8, pp. 6286–6296, Aug. 2017, doi: 10.1109/TPEL.2016.2620428.

[18] M. W. K. Mbukani and N. Gule, "Comparison of high-order and second-order sliding mode observer based estimators for speed sensorless control of rotor-tied DFIG systems," *IET Power Electron.*, vol. 12, no. 12, pp. 3231–3241, Sep. 2019, doi: 10.1049/iet-pel.2018.6225.

[19] M. Benbouzid, B. Beltran, H. Mangel, and A. Mamoune, "A high-order sliding mode observer for sensorless control of DFIG-based wind turbines," in *Proc. IEEE IECON - 38th Annu. Conf. Ind. Electron. Soc.*, 2012, pp. 4288–4292, doi: 10.1109/IECON.2012.6389200.

[20] D. D. Reigosa, F. Briz, C. Blanco, and J. M. Guerrero, "Sensorless control of doubly fed induction generators based on stator high-frequency signal injection," *IEEE Trans. Ind. Appl.*, vol. 50, no. 5, pp. 3382–3391, Sep./Oct. 2014, doi: 10.1109/TIA.2014.2303255.

[21] D. D. Reigosa, F. Briz, C. B. Charro, A. Di Gioia, P. García, and J. M. Guerrero, "Sensorless control of doubly fed induction generators based on rotor high-frequency signal injection," *IEEE Trans. Ind. Appl.*, vol. 49, no. 6, pp. 2593–2601, Nov./Dec. 2013, doi: 10.1109/TIA.2013.2264271.

[22] B. K. Tshiloz, D. Vilchis-Rodriguez, S. Djukanović, N. Sarma, and S. Djurović, "Sensorless speed estimation in wound rotor induction machines by spectral search of the stator phase power signal," *IET Elect. Power Appl.*, vol. 10, no. 6, pp. 581–592, Jul. 2016, doi: 10.1049/iet-epa.2015.0513.

[23] A. Wang, S. Dukanović, N. Sarma, and S. Djurović, "Implementation and performance evaluation of controller signal embedded sensorless speed estimation for wind turbine doubly fed induction generators," *Int. J. Elect. Power Energy Syst.*, vol. 148, Jun. 2023, Art. no. 108968.

[24] K. Blecharz, D. Wachowiak, and Z. Krzemiński, "A novel speed observer for doubly-fed induction generator," in *Proc. 19th Eur. Conf. Power Electron. Appl.*, 2017, pp. P.1–P.10.

[25] D. G. Forchetti, G. O. Garcia, and M. I. Valla, "Adaptive observer for sensorless control of stand-alone doubly fed induction generator," *IEEE Trans. Ind. Electron.*, vol. 56, no. 10, pp. 4174–4180, Oct. 2009, doi: 10.1109/TIE.2009.2014907.

[26] R. Bhattarai, N. Gurung, A. Thakallapelli, and S. Kamalasadan, "Reduced-order state observer-based feedback control methodologies for doubly fed induction machine," *IEEE Trans. Ind. Appl.*, vol. 54, no. 3, pp. 2845–2856, May/Jun. 2018, doi: 10.1109/TIA.2018.2797252.
[27] S. Yang and V. Ajjarapu, "A speed-adaptive reducedorder observer for sensorless vector control of doubly fed induction generator-based variable-speed wind turbines," *IEEE Trans. Energy Convers.*, vol. 25, no. 3, pp. 891–900, Sep. 2010.
[28] G. Brando, A. Dannier, and I. Spina, "Performance analysis of a full order sensorless control adaptive observer for doubly-fed induction generator in grid connected operation," *Energies*, vol. 14, no. 5, Feb. 2021, Art. no. 1254.
[29] K. Xiahou, M. S. Li, Y. Liu, and Q. H. Wu, "Sensor fault tolerance enhancement of DFIG-WTs via perturbation observer-based DPC and two-stage Kalman filters," *IEEE Trans. Energy Convers.*, vol. 33, no. 2, pp. 483–495, Jun. 2018, doi: 10.1109/TEC.2017.2771250.
[30] M. Morawiec, K. Blecharz, and A. Lewicki, "Sensorless rotor position estimation of doubly fed induction generator based on backstepping technique," *IEEE Trans. Ind. Electron.*, vol. 67, no. 7, pp. 5889–5899, Jul. 2020, doi: 10.1109/TIE.2019.2955403.
[31] B. Bossoufi, M. Karim, A. Lagrioui, M. Taoussi, and A. Derouich, "Observer backstepping control of DFIG-generators for wind turbines variable-speed: FPGA-based implementation," *Renewable Energy*, vol. 81, 2015, pp. 903–917.
[32] M. Morawiec, K. Blecharz, and A. Lewicki, "Non-adaptive speed and position observer of doubly-fed induction generator," in *Proc. IEEE Int. Conf. Elect. Mach.*, 2022, pp. 1744–1749.
[33] V. Lakshmikantham, S. Leela, and A. A. Martynyuk, *Practical Stability of Nonlinear Systems*. Singapore: World Sci. 1990.
[34] R. Cárdenas, R. Peña, J. Clare, G. Asher, and J. Proboste, "MRAS observers for sensorless control of doubly-fed induction generators," *IEEE Trans. Power Electron.*, vol. 23, no. 3, pp. 1075–1084, May 2008.

Marcin Morawiec (Senior Member, IEEE) received the M.Sc. degree from the Czestochowa University of Technology, Czestochowa, Poland, in 2003, and the Ph.D. and D.Sc. degrees from the Gdansk University of Technology, Gdansk, Poland, in 2007 and 2017, respectively, all in electrical engineering.

Since 2017, he has been an Associate Professor with the Department of Electric Drives and Energy Conversion with the Gdansk University of Technology. He has authored more than 70 articles, two monographs, two chapters in books, Polish patent, and five patent applications. His research interests include multiscalar models, nonlinear control of any electrical machines, sensorless control, nonlinear control, backstepping control, adaptive observer backstepping, and sliding mode.

Krzysztof Blecharz received the M.Sc. degree in electrical engineering from the Czestochowa University of Technology, Czestochowa, Poland, in 2002 and the Ph.D. degree in electrical drives from the Gdansk University of Technology, Gdansk, Poland, in 2008.

Since 2008, he has been an Adjunct with Gdansk University of Technology. He is the author of more than 15 articles, one Polish patent, and participant in many research projects as designer or researcher. His main scientific activities are concentrated on doubly-fed generator control systems, multiscalar models of electrical machines, sensorless control, and nonlinear control in electric drives.